Tribology International 159 (2021) 106952

Contents lists available at ScienceDirect

Tribology International

journal homepage: http://www.elsevier.com/locate/triboint

Tribological mechanism of (Cr, V)N coating in the temperature range of 500–900 °C

Cuicui Wang [a,b], Beibei Xu [a], Zhenyu Wang [a,b,**], Hao Li [a], Li Wang [a], Rende Chen [a], Aiying Wang [a,b,***], Peiling Ke [a,b,*]

[a] Key Laboratory of Marine Materials and Related Technologies, Zhejiang Key Laboratory of Marine Materials and Protective Technologies, Ningbo Institute of Materials Technology and Engineering, Chinese Academy of Sciences, Ningbo, 315201, China
[b] Center of Materials Science and Optoelectronics Engineering, University of Chinese Academy of Sciences, Beijing, 10049, China

ARTICLE INFO

Keywords:
(Cr, V)N coatings
High-temperature friction
Wear mechanism
Oxidation

ABSTRACT

Aiming to study the influence of temperature on the wear mechanism, we fabricated (Cr, V)N coating by cathodic arc ion-plated and conducted tribological experiments at 500–900 °C. The results indicated that there were two tribological behaviors, depending on the temperature. Below 600 °C, the (Cr, V)N coatings exhibited a high friction coefficient, but generated a mild wear because of the slight oxidation. Above 700 °C, the increased oxidation degree reduced adhesion of asperity contacts. However, the wear rate enhanced significantly with the temperature increasing from 700 to 900 °C due to the fast oxidation accompanied by the decrease in both hardness and adhesion strength.

1. Introduction

With the development of modern high speed machining and molding industries, transition metal nitride (TMN) hard coatings with good tribological performance at a wide range of temperatures are desired to meet the engineering application [1–4]. As a kind of representative TMN hard coatings, chromium nitride (CrN) coatings have occupied an important position in the cutting tool industry for more than two decades, because of their good oxidation resistance, anti-corrosion, and anti-adhesive properties, etc [5–7]. However, the poor tribological performance and relatively low hardness are still the open challenges for CrN coatings, especially the limited application over 550 °C under dry condition [8–10]. Taking into the solid solution effect, in our previous work, Vanadium (V) element was incorporated into the CrN coatings to form solid solution (Cr, V)N coatings [11]. The results showed the (Cr, V)N coating exhibited the superior hardness (20 GPa) and resistance to sliding wear (wear rate 2.5×10^{-7} $mm^3N^{-1}m^{-1}$), together with a lower friction coefficient at 0.26 using the Al_2O_3 ball counterpart with sliding speed at 0.5 m/s and load at 5 N at room temperature.

Recently, series V-based hard coatings has attracted increasing interests because they can maintain relatively low friction coefficient at a wide range of temperatures owning to the emergence of Magnéli-phase oxides [12–14]. For VN coatings, oxidation started at around 500 °C with the formed Magnéli-phase oxides, which benefited the continuous decrease in friction coefficient at temperatures above 500 °C until reaching a value of 0.25 at 700 °C [15]. The wear tests of TiAlN/VN multilayer coatings (V~50 at.%) against Al_2O_3 demonstrated a decrease of friction coefficient from 0.55 at 25 °C to 0.18 at 700 °C [16]. In addition, the tribological measurement of $(Cr_{0.59}Al_{0.21}V_{0.2})N$ coatings against the same steel showed that due to the appearance of V_3O_7, the COF decreased from 0.6 at 25 °C to 0.05 at 800 °C [17]. It could be said that the oxidation of V element being Magnéli-phase oxides at elevated temperatures for the V-based coatings is beneficial for providing lubricious effects arisen from their easy crystallographic shear feature.

However, the rapid oxidation of V occurring at elevated temperatures for the V-based coatings could deteriorate the wear resistance

* Corresponding author. Key Laboratory of Marine Materials and Related Technologies, Zhejiang Key Laboratory of Marine Materials and Protective Technologies, Ningbo Institute of Materials Technology and Engineering, Chinese Academy of Sciences, Ningbo, 315201, China.
** Corresponding author. Key Laboratory of Marine Materials and Related Technologies, Zhejiang Key Laboratory of Marine Materials and Protective Technologies, Ningbo Institute of Materials Technology and Engineering, Chinese Academy of Sciences, Ningbo, 315201, China.
*** Corresponding author. Key Laboratory of Marine Materials and Related Technologies, Zhejiang Key Laboratory of Marine Materials and Protective Technologies, Ningbo Institute of Materials Technology and Engineering, Chinese Academy of Sciences, Ningbo, 315201, China.
E-mail addresses: wangzy@nimte.ac.cn (Z. Wang), aywang@nimte.ac.cn (A. Wang), kepl@nimte.ac.cn (P. Ke).

https://doi.org/10.1016/j.triboint.2021.106952
Received 14 December 2020; Received in revised form 8 February 2021; Accepted 21 February 2021
Available online 24 February 2021

Table 1
Chemical composition of the substrate and coating materials (at.%).

Material	Fe	Si	Cr	Mn	Ni	C	V	N
Substrate	89.67 ±0.045	0.74 ±0.035	1.76 ±0.025	1.41 ±0.36	0.54 ±0.37	5.88 ±0.095	–	–
Coating	–	–	57.84 ±0.66	–	–	–	14.34 ±0.23	27.83 ±0.89

Table 2
The detailed process parameters of prepared CrVN coating.

Process	Bias Voltage (V)	Current (A)			Chamber Pressure (mtorr)	Ar Flow (mL/min)	N_2 Flow (mL/min)	Deposition Time (min)
		Ion Beam	Cr Cathode	$Cr_{75}V_{25}$ Cathode				
Etching	−100	0.2	–		–	40	–	60
Cr layer	−200	–	50	–	25	200	–	8
CrN layer	−60	–	50	–	50	–	550	8
CrVN layer	−80	–	–	50	70	–	550	150

because of the V out-diffusion [12]. Mu et al. [18] studied the adaptive lubricious behavior of VN-VN/Ag multilayer coating from 25 °C to 700 °C. They found the coating showed excellent adaptive lubrication properties, and the coefficient of friction decreased with increasing temperature. But the wear rate increased drastically beyond 500 °C because of oxidization and a tribo-chemical reaction. The VN coatings with two kinds of vanadium oxide (V_2O_5 and VO_2) pre-oxide layers were manipulated by different oxidation treatments at 600 °C according to the report of Cai et al. [19]. The VN coatings containing a pre-oxide layer of V_2O_5 possessed the lowest COF but the largest wear rate, while they behaved a relatively low COF and wear rate with a pre-oxide layer of VO_2 when compared to that without pre-oxide layer. Furthermore, Lewis et al. [20] investigated the oxidation behavior of TiAlN/VN superlattice coating in air, where the V_2O_5 oxide was visible on the surface at 600 °C. However, the coating was destroyed to form the complicated oxide products composed of Fe, V, Ti, Al and oxygen at 700 °C. It is thus clear that oxidation behavior is an important factor determining the wear resistance of V-based hard coatings. Therefore, it is of great necessary to gain insight into the wear mechanism of V-based coatings and the relationship with oxidation resistance at temperatures beyond of 500 °C.

In this work, (Cr, V)N solid solution coatings with a V content of 14 at.% were successfully fabricated by the home-made cathodic arc technique. The oxidation together with wear behaviors of (Cr, V)N coatings were studied in detail at temperatures from 500 °C to 900 °C. Importantly, we did not only assess the individual mechanical and oxidation properties of (Cr, V)N coatings, but also discuss the wear mechanism in terms of the microstructure evolution during friction test.

2. Experimental methods

2.1. Coating deposition

The substrate materials used in this research were iron-based high temperature alloy disks (Φ25 mm × 3 mm) for wear and oxidation tests, and the Al_2O_3 substrate with size of 5 mm × 5 mm × 0.5 mm was employed for thermal-gravimetric analysis (TGA). The precise composition of the alloy is shown in Table 1. Prior to the deposition, the substrates were ultrasonically cleaned with acetone and alcohol for 10 min, respectively, and then placed on the vertical rotating holder with a rotation speed of 9.5 rpm facing to the targets.

The (Cr, V)N coatings were deposited by a home-made cathodic arc evaporation system. The deposition process was carried out in pure N_2 atmosphere at 450 °C. Cr target (purity: 99.99 wt%; size: Φ128 mm × 15 mm) and CrV composite target (purity: 99.9 wt%; size: Φ128 mm × 15 mm) with the atomic ratios of 75: 25 were used for the deposition of Cr, CrN interlayer and (Cr, V)N coatings, respectively. Two targets were pre-sputtered for 5 min and the substrates were etched by Ar^+ bombardments for 60 min before deposition so as to remove the contaminants adsorbed on the surface. Cr and CrN interlayers were deposited for 8 min, respectively, at coating/substrate interface to favor the adherence of the coatings. Then (Cr, V)N coatings were deposited for 150 min in pure N_2 atmosphere at 70 mtorr. Detailed process parameters are shown in Table 2. The coating composition listed in Table 1 revealed that the V content was lower than that in the target, causing higher Cr content, which was likely due to the effect of preferential re-sputtering of V during the growth. The total thickness of the (Cr, V)N coating in this study was controlled around 4.5 μm.

2.2. Tribological and oxidation tests

The tribological behavior of (Cr, V)N coatings was studied with a ball-on disk tribometer (Anton Paar THT) operating at dry-sliding test with various elevated temperatures including 500 °C, 600 °C, 700 °C, 800 °C and 900 °C. The friction counterpart was Al_2O_3 ball (Φ 6 mm). The normal load, sliding speed, sliding distance and radius of the wear track were kept at 5 N, 5 cm/s, 100 m and 5 mm, respectively. Normalized wear rates (W_R, $mm^3N^{-1}m^{-1}$) are calculated using the following equation [21]:

$$WR = \frac{d(3d^2 + 4b^2)2\pi r}{6bF_nL}$$

where d is the depth of the wear track and b is the width of the wear track, which are determined by a surface profilometer (Alpha-Step IQ, America), r is the radius of the wear track, F_n is the normal load and L is the sliding distance. In order to reduce the measurement error, the wear rate of each sample was calculated at least five times by selecting different positions within the wear track.

The oxidation test was conducted at the same targeted temperatures (500 °C, 600 °C, 700 °C, 800 °C and 900 °C) in a tube furnace as friction test. The tube furnace was heated to the oxidation temperature at the rate of 10 °C/min under the atmospheric environment and the coatings were oxidized for 30 min, which were chosen to match the parameters of the tribo-tests.

2.3. Characterization techniques

Scanning electron micrographs and chemical composition of the as-deposited coatings and substrate as well as the coatings after oxidation and friction tests were carried out by a field emission FEI Quanta FEG 250 scanning electron microscope (SEM) equipped with an energy dispersive spectrometer (EDS). X-ray diffraction (XRD) measurements were used to detect the phase in the coating after oxidation, using the Kα

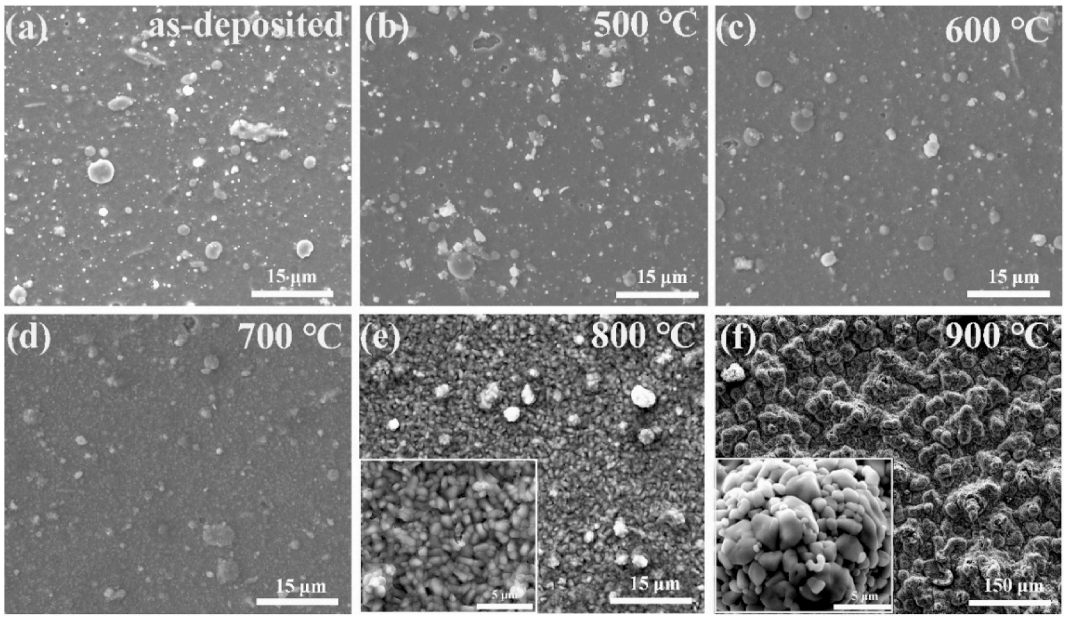

Fig. 1. Surface morphologies of the(a) as-deposited coating, and coatings after oxidation at (b) 500 °C, (c) 600 °C, (d) 700 °C, (e) 800 °C, (f) 900 °C.

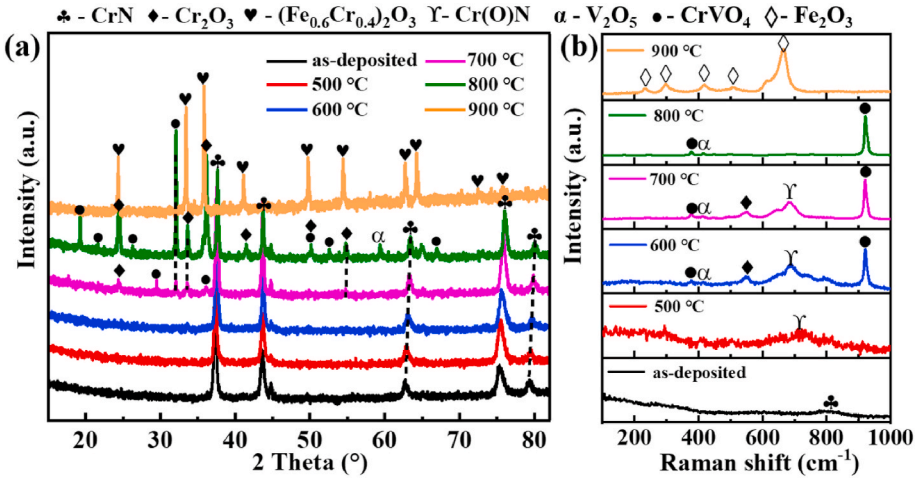

Fig. 2. (a) XRD patterns and (b) Raman spectra of as-deposited (Cr, V)N coating and coatings oxidized in ambient air from 500 °C to 900 °C.

radiation of a Cu filament with a Bruker D8 Advance diffractometer. TGA was performed using PerkinElmer Diamond TG/DTA equipment with the temperature program ranging from 25 °C to 900 °C (heating rate 10 °C/min) in flowing air. The Raman spectra (In Via-reflex, Renishaw) of the surface after oxidation and wear track after tribology were obtained with a 532 nm exciting wavelength laser. The laser power for this research was low enough to prevent changing the structure of the coating's surface. Additionally, after the oxidation test, the hardness and adhesion strength were measured to evaluate the mechanical properties. The hardness (H) was tested by MTS nanoindentation system equipped with a 20-nm-radius Berkovich diamond tip using continuous stiffness mode, and the coating surface was polished in advance to minimize the measurement error. The CSM scratch tester equipped with a tapered diamond tip with a radius of 0.2 mm and a cone angle of 120° was used to test the load bearing capacity of the coatings. The tip moved at a speed of 1.5 mm/min for a distance of 3 mm. At the same time, the applied load linearly increased from 0 N to 100 N with a loading speed of 50 N/min. The load where the coating is completely peeled off is determined to be the adhesion strength between the coating and the substrate.

Three-dimensional (3D) cross sectional profile of the wear tracks were carried out by scanning white light interference microscope (3D Universal Profilometer, Rtec). For further analysis, the TEM samples of cross-sectional profiles of the wear tracks were prepared by a focused ion beam (FIB, Auriga, Germany). The element distribution and microstructures were characterized by STEM and high-resolution TEM (HRTEM, Talos F200X, USA).

3. Results

3.1. Oxidation behavior between 500 and 900 °C

3.1.1. Composition and microstructure characteristics

The surface morphologies of the (Cr, V)N coatings after oxidization at different temperatures are reported in Fig. 1. The XRD and Raman spectra analyses of (Cr, V)N coating oxidized at different temperatures in ambient air are carried out in Fig. 2. Fig. 1a–c shows that the coatings with similar smooth surface morphology and large roundish macrograin particles, which is the typical characteristic of the arc evaporation deposition method. Noted that the coatings oxidized at 500 °C also possessed the similar phase composition to that of as-deposited (Cr, V)N

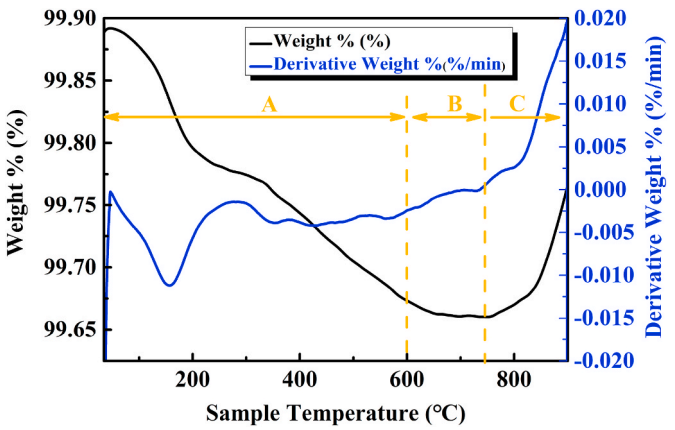

Fig. 3. The TGA curve of (Cr, V)N coating tested in ambient air from room temperature to 900 °C.

coating from the XRD and Raman spectra (Fig. 2), indicating that the (Cr, V)N coating was stable and unoxidized. After 600 °C oxidation (Fig. 1c), although the coating retained its original surface morphology, the sporadic white particles appeared in the surface, implying the (Cr, V)N coating started to oxide. As seen in Fig. 2b, the formation of $CrVO_4$ and Cr_2O_3 phases was observed in the Raman spectrum. But differently, only the peaks of CrN phase were shown in XRD spectrum (Fig. 2a), no oxide was observed. This was probably due to the fact that the $CrVO_4/Cr_2O_3$ mixed oxides were in the form of amorphous phase [22]. Further increasing the temperature, the white particles blossomed into discontinuous fine lamellar oxides embedding in the surface and large oxide grains formed at the particles. The oxides such as V_2O_5, $CrVO_4$ and Cr_2O_3 were observed in both XRD and Raman spectra, revealing that the surface oxidized slightly. When the oxidation temperature reached to 800 °C (Fig. 1e), the oxides grew rapidly and the surface was densely overspread with capsule-shaped particles. According to the results in Fig. 2, there were more and stronger peaks of V_2O_5, $CrVO_4$ and Cr_2O_3. At 900 °C, the surface of the coating became more granular and rougher, and was loosely stacked with large cauliflower-shaped particles with different sizes as shown in Fig. 1f, which were formed by chromium and iron oxides (Fig. 2). Besides, it was noted that no CrN peak existed in the coating at 900 °C. This indicated the (Cr, V)N coating oxidized completely, the coating structure was greatly damaged, and the basal elements diffused into the coating and were oxidized.

TGA was further performed on Al_2O_3 substrate to investigate the thermal behavior of (Cr, V)N coating. Fig. 3 presents the TGA curve for (Cr, V)N coating heated from room temperature to 900 °C. The trend of the mass change was observed from the first derivative curve of the TGA curve. It showed that a rapid total mass loss in the TGA curve from room temperature to 600 °C (area A), which might be related to the dissipation of the absorbed water in the (Cr, V)N coating. After that, in area B, due to the release of the small amount of N_2 and the preliminary formation of oxides layers (based on the analyses of XRD, Raman and EDS), the mass loss was alleviated with the increasing temperature up to a certain temperature beyond which a sharp increase occured (area C). This steep increase in total mass was attributed to the complete oxidation of (Cr, V)N into Cr_2O_3.

In order to further study the effects of oxidizability, the cross-sectional morphology after oxidation and the corresponding EDS line scans were characterized. From the cross-sectional morphology of the as-deposited coating, the Cr and CrN interlayers and the coating of ~4 μm thick were obviously distinguished (Fig. 4a). Perpendicular to the surface, there was no changes in the coating thickness oxidized at 500 °C (Fig. 4b). As shown in Fig. 4c, due to the limited accuracy of the line scan technique, even no oxidation layer was detected in the coating at 600 °C, but the coating thickness increased to about 5 μm. According to the

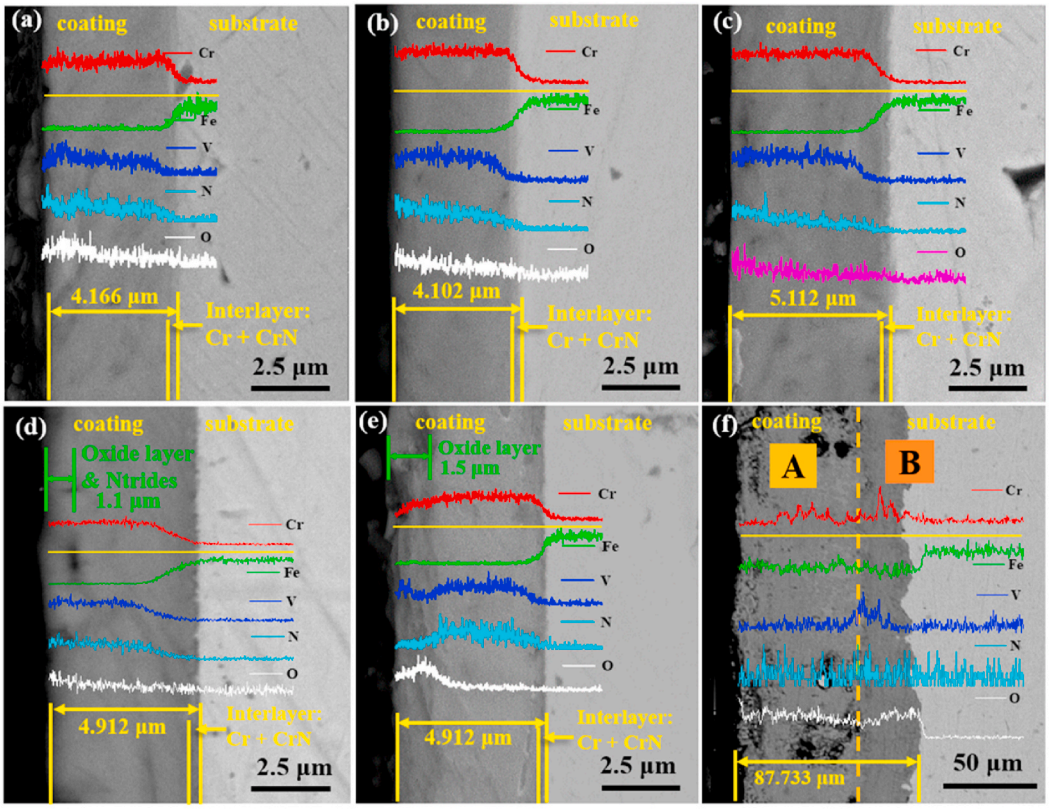

Fig. 4. Backscattered scanning electron microscopy and the corresponding EDS line scans of the cross sections of the (a) as-deposited coating, and oxidized (Cr, V)N coating at (b) 500 °C, (c) 600 °C, (d) 700 °C, (e) 800 °C, (f) 900 °C.

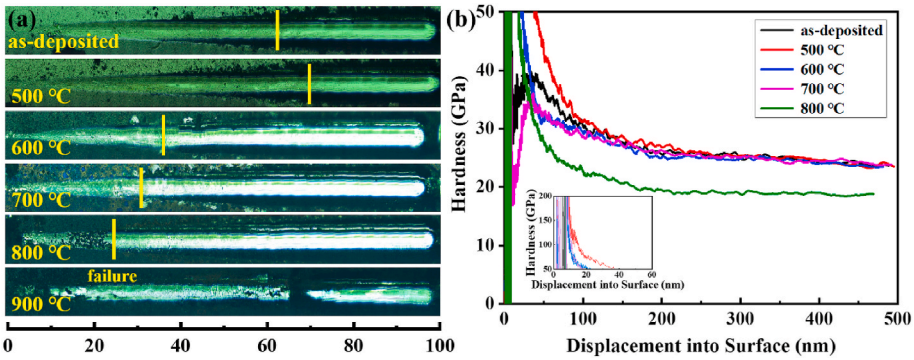

Fig. 5. The (a) scratch morphologies and (b) nano indentation hardness-displacement curves of the as-deposited (Cr, V)N coating and coatings oxidized in ambient air from 500 °C to 900 °C, respectively.

phase composition of the surface and Raman spectra analysis as well as the TGA test, O element started to enter into the coating, and the amorphous Cr_2O_3 and $CrVO_4$ phases were formed, which caused the augment of the coating thickness. At 700 °C (Fig. 4d), a typical scale including mixed oxides (Cr_2O_3, V_2O_5, $CrVO_4$) and nitrides with the thickness of ~1.1 μm was formed on the surface. When the temperature rose to 800 °C, the coating surface was completely oxidized, and a mixed oxide layer (~1.5 μm) containing Cr_2O_3, V_2O_5, $CrVO_4$ and a small amount of Fe_2O_3 were observed (Fig. 4e). The coating totally oxidized at 900 °C and was mainly occupied with iron oxides and a small amount of chromium oxides. After oxidization, the (Cr, V)N coating became loose and porous. The thickness was about 88 μm, almost 22 times larger than that of the as-deposited coating (Fig. 4f). The sharp enhancement in oxide thickness was mainly due to an increase in both the inward diffusion rate of O and outward diffusion rate of Fe as well as the rapid depletion of V and Cr.

3.1.2. Mechanical properties

The progressive load scratch test of the (Cr, V)N coating oxidized at different temperatures was evaluated by the CSM Instruments Revetest equipped with a tapered diamond tip with a radius of 0.2 mm and a cone angle of 120°. In this experiment, the normal load range was 0–100 N, the scratch length was 3 mm and the speed of loading force was 50 N/min. Kinbara et al. [23] suggested that the spallation of the coating occurred during the scratch test, when the strain energy accumulation in the film compressed by the stylus overcame its adhesion energy. Usually, the complete spallation of the coating is referred to the adhesion strength of coating. Based on the spallation of the coating, the adhesion strength was scaled, which was about 62 N, 69 N, 35 N, 32 N and 23 N for as-deposited coating and oxidized coating under 500 °C, 600 °C, 700 °C and 800 °C, respectively (Fig. 5a). Surprisingly, the coating after oxidizing at 900 °C thoroughly failed at the initial stage of scratch test.

It could be concluded that the change of adhesion strength was closely related to the oxidation degree of the coating. With the increase of temperature, the (Cr, V)N coating was oxidized more severely, leading to the poor adhesion of the coating. Above 600 °C, the initial oxidation temperature of the (Cr, V)N coating, a large amount of oxygen entered into the coating and the original structure of the coating was destroyed. Under the condition of high temperature oxidation, the adhesion strength of the coating dramatically decreased when the temperature rose to 600 °C. As further increasing the temperature, the coating underwent a transition from incomplete oxidation to complete oxidation. The adhesion strength was weakened as a consequent of the loose structure.

Fig. 5b illustrated the hardness of as-deposited (Cr, V)N coating and the coatings oxidized at different temperatures. Exceptionally, the coating oxidized at 900 °C failed during the hardness test, so the result was absent. The as-deposited (Cr, V)N coating and the coatings oxidized at 500 °C, 600 °C, 700 °C showed almost the same hardness of 24 GPa,

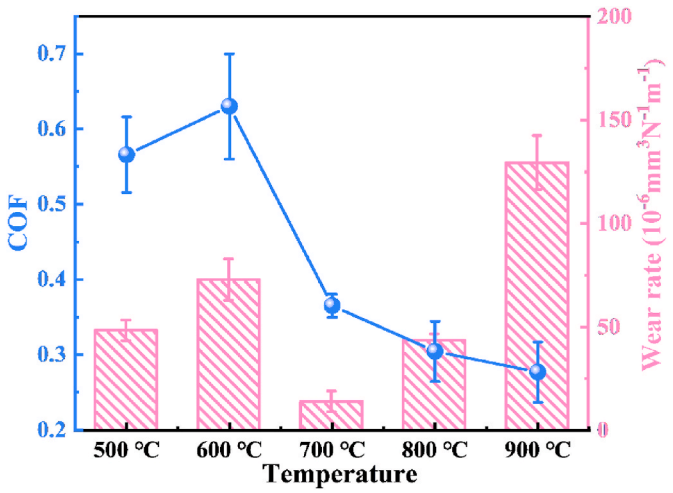

Fig. 6. Friction coefficient and wear rate of (Cr, V)N coating after ball-on-disk friction test performed at temperatures ranged from 500 °C to 900 °C.

while the hardness of 19 GPa was obtained for the coating of 800 °C, which was obviously lower compared to other samples. CrN phase was the main phase at 500 °C and no oxidation phenomenon occurred. At 600 °C, oxygen began to diffuse into the coating but the hardness and main phase composition of the coating were still maintained. At 700 °C, the coating's surface incompletely oxidized, and the CrN phase as the main phase component played a major role in the deteriorated mechanical properties. When the temperature increased to 800 °C, the coating's surface completely oxidized and was covered by a mixed oxide layer. The dissipation of the CrN phase and the increasingly loose structure caused a great loss of the hardness at 800 °C than samples oxidized at other temperatures.

It is conclusive that, the oxidation rate increased with increasing temperature over 600 °C. The structure of the coating became looser and accompanied by the breaking down of the adhesion strength. The hardness of the coating was also damaged by the dissipation of CrN main phase. Therefore, the mechanical properties of the coating decreased with the oxidation temperature increasing.

3.2. Tribological performances between 500 and 900 °C

Fig. 6 shows the average friction coefficient (COF) and wear rate of (Cr, V)N coating at various temperatures from 500 °C to 900 °C. The COF increased slightly from 0.57 to 0.63 with the temperature increased from 500 °C to 600 °C. However, the COF obviously decreased with the temperature increased from 700 °C to 900 °C, which might be ascribed to the formation of lubricating oxide phase. Specifically, the COF of

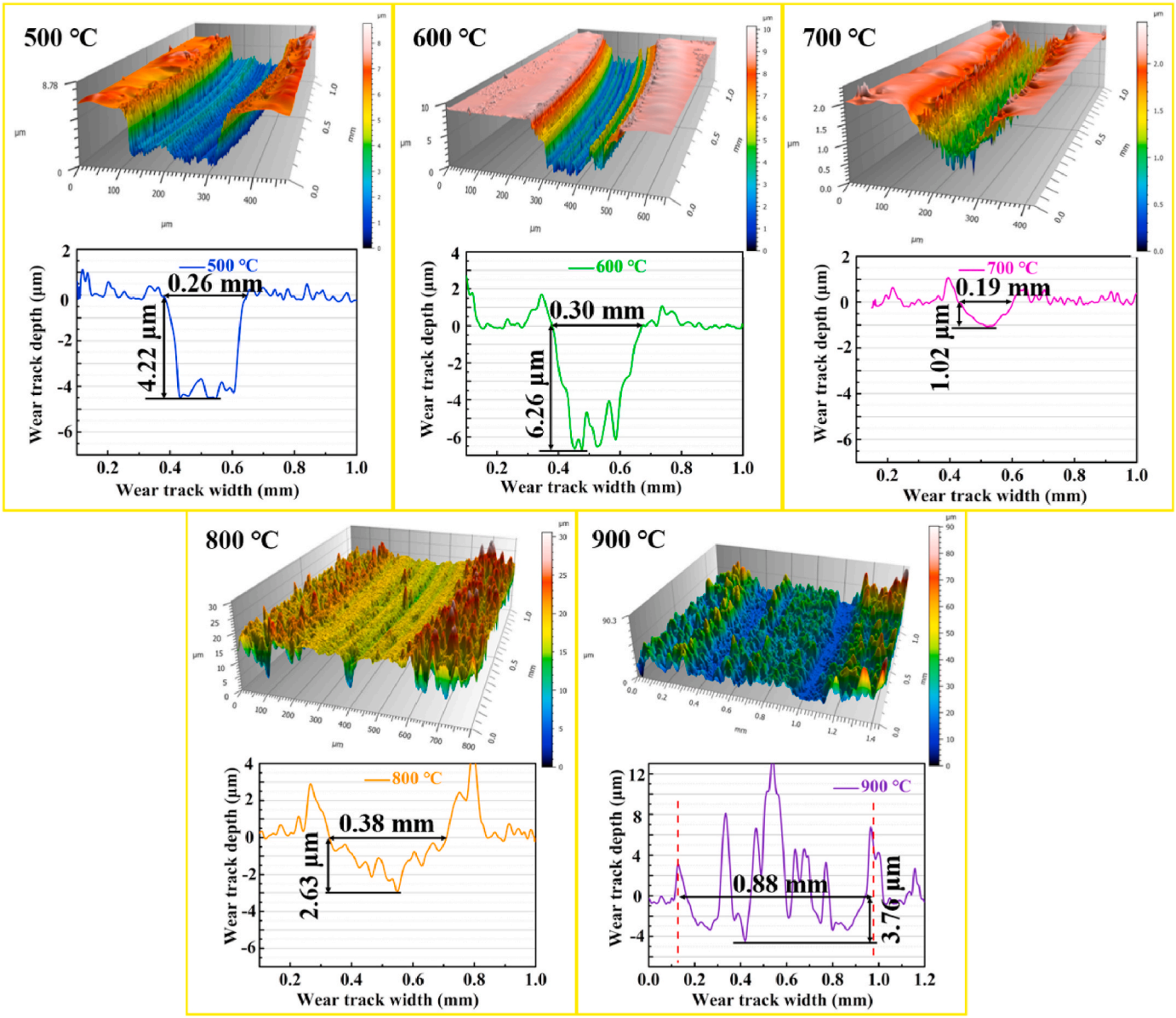

Fig. 7. The comparison of 3D cross-sectional profiles of the wear tracks at various temperatures and the corresponding 2D wear track depth profiles were attached below.

coating was 0.37 at 700 °C, which was 41.3% lower than that of 600 °C. At 900 °C, the COF reached the lowest value of 0.28. According to the two-dimensional (2D) depth profiles of the wear track tested by the surface profilometer, an increase in wear rate from $(4.83 \pm 0.5) \times 10^{-5}$ $mm^3N^{-1}m^{-1}$ to $(7.29 \pm 1.0) \times 10^{-5}$ $mm^3N^{-1}m^{-1}$ was observed as temperature varied from 500 °C to 600 °C. The coating at 700 °C exhibited the lowest wear rate of $(1.4 \pm 0.5) \times 10^{-5}$ $mm^3N^{-1}m^{-1}$, indicating the excellent anti-wear resistance. At temperature of 800 °C, the wear rate of coating was $(4.36 \pm 0.3) \times 10^{-5}$ $mm^3N^{-1}m^{-1}$, almost an order of magnitude lower than $(12.9 \pm 1.3) \times 10^{-5}$ $mm^3N^{-1}m^{-1}$ at 900 °C.

Fig. 7 displays the 3D and the corresponding 2D cross-sectional profiles of wear tracks after friction tests performed at different temperatures. The width and depth marked in the 2D profiles were the average values measured at different positions of the wear track. The wear track at 500 °C was 0.26 mm width and 4.22 μm deep. In comparison, the wear track at 600 °C was 2 μm deeper than that of 500 °C, which was far beyond the thickness of the as-deposited (Cr, V)N coating. Moreover, the center of the wear track dented apparently and was full of rough furrows paralleling to the sliding direction. In contrast, the formation of oxide layers at 700 and 800 °C, as shown in Fig. 4g and h, contributed to unignored improvement of the tribology performance. The depth of the wear track was 1.02 μm and 2.63 μm, respectively, for 700 °C and 800 °C, indicating the slight wear of the coatings. When the temperature increased to 900 °C, the coating completely oxidized and the structure of oxides were not dense enough to tolerant any force. As a result, the sample of 900 °C showed the highest wear rate compared to other researched temperatures. As it worn out, the wear track was much wider and the outgrowing oxides scattered in the center of the wear track.

In order to address the wear mechanism, the morphology of the wear tracks was evaluated by SEM, as shown in Fig. 8. The EDS elemental composition as well as Raman spectra in different areas (labeled in SEM micrograph) are displayed in Table 3 and Fig. 9. In particular, the evolution of comprehensive worn surface was discussed. The wear track of 500 °C revealed a smooth plane. Neither Fe nor Mn were detected in the analyses of EDS results, which showed the remained intact interface to the substrate. Raman spectra revealed the CrN phase as the main part

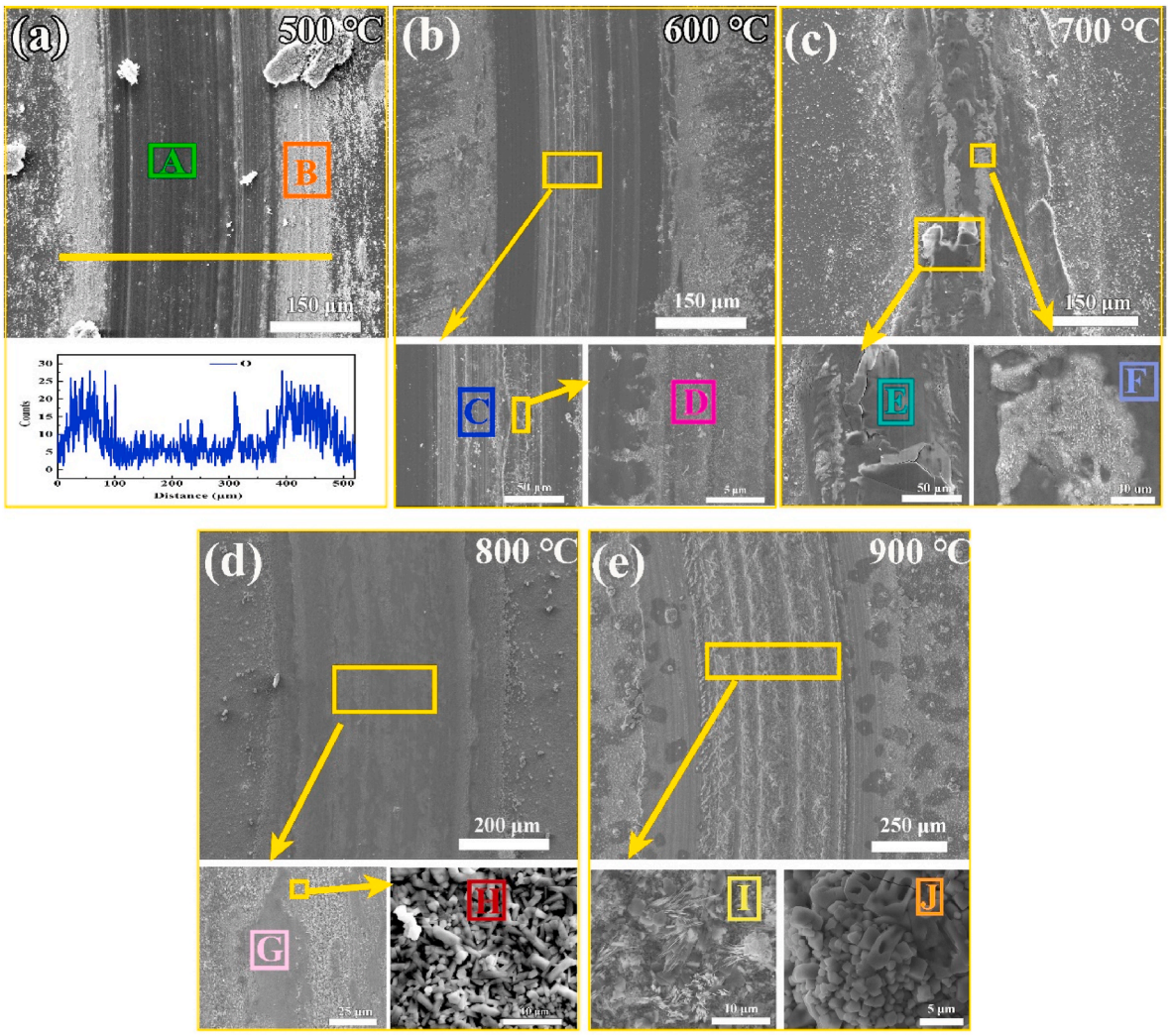

Fig. 8. SEM micrograph of wear tracks and partial enlarged details: (a) 500 °C, (b) 600 °C, (c) 700 °C, (d) 800 °C, (e) 900 °C.

Table 3
The element composition at different positions of wear tracks (corresponding to the letter number in Fig. 8).

Sample ID	Elemental Composition (at.%)					
	Cr	V	N	O	Fe	Mn
A-500 °C	41.34 ±0.75	9.33 ±0.60	44.76 ±0.60	4.57 ±0.22	–	–
B-500 °C	39.09 ±0.05	9.88 ±0.16	21.44 ±0.27	29.59 ±0.06	–	–
C-600 °C	29.57 ±0.34	2.71 ±0.22	8.16 ±0.72	23.73 ±0.53	35.83 ±0.15	–
D-600 °C	6.15 ±1.23	–	–	30.65 ±7.03	63.20 ±5.47	–
E−700 °C	39.68 ±1.55	11.75 ±0.80	16.78 ±2.06	31.79 ±0.75	–	–
F-700 °C	7.01 ±0.21	2.03 ±0.33	–	43.12 ±3.24	47.84 ±3.54	–
G-800 °C	34.92 ±0.87	2.27 ±0.14	–	55.65 ±0.58	5.53 ±0.04	–
H-800 °C	19.95 ±0.21	14.62 ±2.14	–	49.75 ±4.12	15.68 ±1.77	–
I-900 °C	43.74 ±0.51	17.09 ±0.05	–	23.93 ±3.39	15.24 ±2.83	–
J-900 °C	–	18.23 ±1.05	–	29.01 ±0.87	47.55 ±2.31	5.21 ±1.23

of the wear track, and the oxidation phases, such as V_2O_5, Cr_2O_3, $CrVO_4$, were not detected in the wear track but in wear debris. It could be explained as the Al_2O_3 ball continuously removed ultra-thin oxide formed on the coating during the sliding process and exposed unoxidized coating to the atmosphere without any lubrication phase formed. In this case, the (Cr, V)N coating showed the high COF and wear rate. Increasing the temperature to 600 °C, a wide groove stripe paralleling to the sliding orientation in the middle of the wear track appeared, which was consistent with the result of the 3D morphology. The fish-scale-like patterns featured the groove stripe (a close inspection shown in area C), indicating the occurrence of severe shear deformation of the tribo-film during the wear test. The EDS and Raman spectroscopy analyses confirmed the existence of Fe_2O_3 oxide phase, suggesting that the Al_2O_3 ball locally contacted the substrate. Due to poor adhesion and lack of lubricating oxides, the coating showed poorer tribological properties than 500 °C. The COF at higher temperatures sharply decreased because of a more intensified oxidation and thereby the wear track topography changed. Alongside the wear track of (Cr, V)N coating after testing at 700 °C, a serious accumulation of the wear debris and localized spallation of the coating were observed (area E). Raman spectra of the worn surface mainly showed the Cr(O)N that a small amount of O was dissolved in CrN, and V_2O_5 peaks, in line with the aforementioned thermal study of the coating. It was reported that V_2O_5 had low melting temperature of 685 °C, above which the molten V_2O_5 would lead to a liquid lubrication, and further, to confer a low friction coefficient [24].

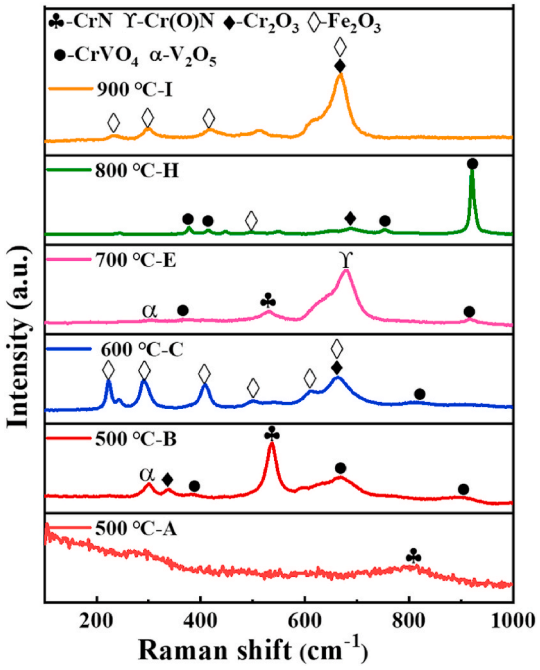

Fig. 9. The Raman spectra at different positions of wear tracks (corresponding to the letter number in Fig. 8).

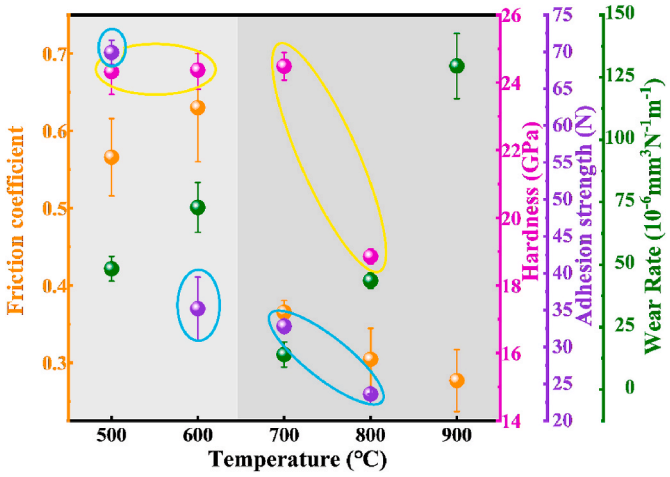

Fig. 10. The tribological and mechanical properties at different temperatures.

However, supported by the EDS analysis of area F, Fe-oxides were present in the form of white rod-like roll, which could be arisen from the oxidation/sublimation of the Fe element in the substrate and pollution of the wear track surface. Due to higher oxidation rate at 800 °C, the worn coating surface was completely covered by oxide platelet (area H). The Raman spectra and EDS analyses suggested its multi-oxide composition, such as $CrVO_4$, Cr_2O_3 and a small fraction of Fe_2O_3. The intermittently dispersed smeared appearance also demonstrated the formation of a soft V–O phase during the friction test (area G) [25]. Therefore, the COF further decreased with the increasing oxidation rate. After that, combined with the result of the oxidation behavior, the coating totally oxidized at 900 °C, and then the wear track topography showed decisive changes. The outgrowing oxide scales agglomerated in the center of the wear track. As a close scrutiny to the oxide scales shown in area I and J, cauliflower-shaped oxides with the dispersed needle-like fine particles were observed. The oxide scales shown in Raman spectroscopy were exclusive of any sign of V–O phase, instead $(Fe, Cr)_2O_3$ as the dominant phases. According to the cross-sectional morphology of isothermal oxidation in Fig. 4f, the V element was subject to dissipate at 900 °C. But this did not rule out the existence of the V–O phase. The EDS result corroborated that there was a spot of V–O phase parceled in the cauliflower-shaped particles.

4. Discussion

In case of high temperature, the oxidation behavior of the coating and the changes of the interfacial mechanical properties play key roles in the tribological properties of the coating. In this work, the dependence of friction in temperature range of 500–900 °C upon the evolution of oxidation and mechanical behaviors of (Cr, V)N coatings was particularly focused. Considering the melting point of V_2O_5 was 685 °C, whether the liquid lubricating phase of V_2O_5 was formed or not at this transition point, the high temperature friction mechanism of the (Cr, V)N coating indicated different changes according to the COF. Based on the above-mentioned characterization, the tribological behaviors of (Cr, V)N system were classified into two parts, as shown in Fig. 10, including high COF of 0.57–0.63 at 500–600 °C and low COF of 0.28–0.37 at 700–900 °C, of which the tribological mechanisms were indicative of mechanical wear and oxidation dependent, respectively.

4.1. Tribological behaviors at 500–600 °C

The feeble Cr_2O_3 and $CrVO_4$ mixed oxides detected by Raman spectra and the increase in thickness of coating observed by the cross-sectional morphology substantiated the oxidation of the (Cr, V)N coating at 600 °C. As the oxidation behavior caused the loss of inherent structure, the adhesion strength was also damaged, as shown in Fig. 10. During the tribology test, the coating at 600 °C shared similar morphology of the wear track to that of 500 °C with marginal lubricious oxides formed, due to the limitation of the oxidation rate. The lubricious oxides were only expected to form at the asperity contacts, therefore their amount was not ample enough to provide effective lubrication. As a consequence, the mechanical wear took place at this temperature interval. A dynamic process of powdering, wear particle generation and self-agglomeration contributed to the high friction and the damage of the adhesion strength at 600 °C which reduced the wear resistance.

4.2. Tribological behaviors at 700–900 °C

At elevated temperatures, the growing oxide scale in Fig. 4 manifested the accelerated oxidation rate of (Cr, V)N coating. The friction behaviors of the coating substantially profited from lubricating oxides. As shown in Fig. 11, the cross-sectional views of the wear tracks together with related elemental mapping after friction tests at 700 °C and 800 °C were examined to further reveal lubrication mechanism. According to the EDS elemental mapping results, the upper layer was assigned to oxide scales with abundance of Cr, V and O, as well as Fe element somehow derived from the substrate, while underlying layer was ascertained to (Cr, V)N coating. It suggested that (Cr, V)N grains had undergone static oxidation beneath the worn wear track, which was also observed in the literature [26]. The compositional distribution of the oxide scale grain boundary at 800 °C was also captured (Fig. 12a). Noted that both the V and Fe agglomerated in the grain boundary, indicating these two elements diffused through the grain boundary. In addition, Fe element passed through the coating and then diffused outward to the oxide scale due to the strong affinity with oxygen. As previously observed by Raman spectra (Fig. 9), the oxide scale was comprised of $CrVO_4$, Cr_2O_3, V_2O_5 and Fe_2O_3, which rendered beneficial lubrication due to their easy shear or breaking bonding.

In case of 700 °C, the oxide structure was visibly dense with no signs of voids or pores and the thickness was measured of 150 nm. It was noted that the darker area in the middle layer of the oxide scale was rich in V, which was confirmed by V elemental distribution contrast

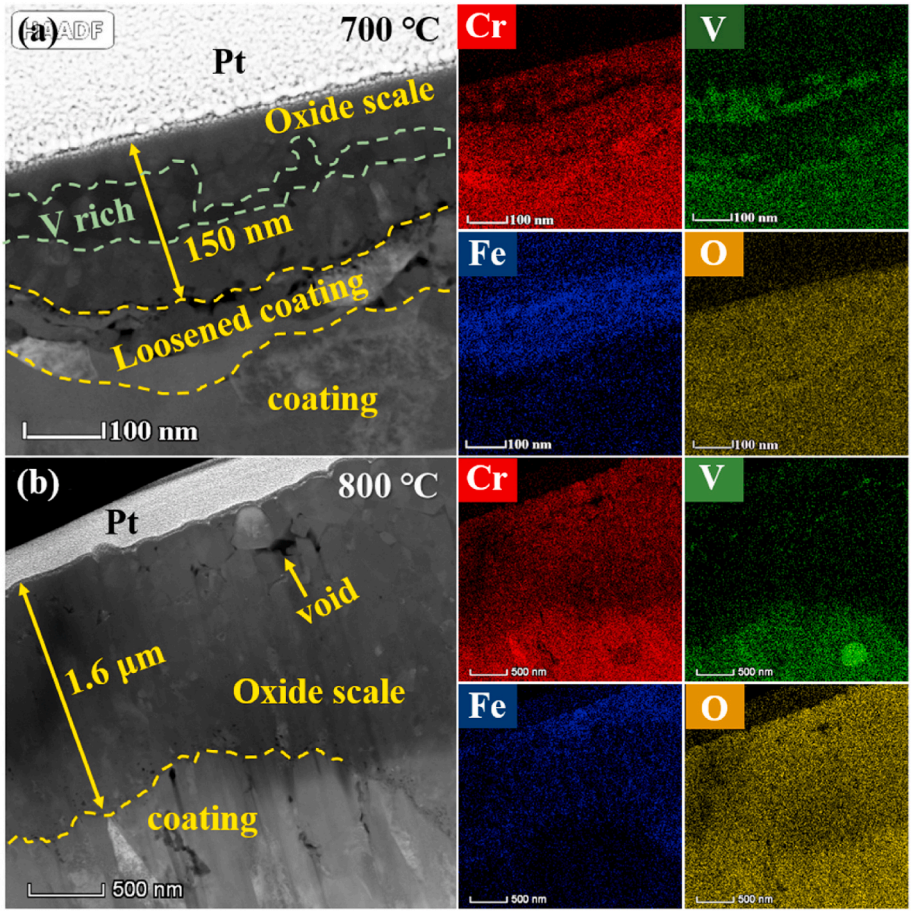

Fig. 11. The cross-sectional STEM images of the wear track at (a) 700 °C and (b)800 °C, and the corresponding EDS mapping images of Cr, V, Fe and O.

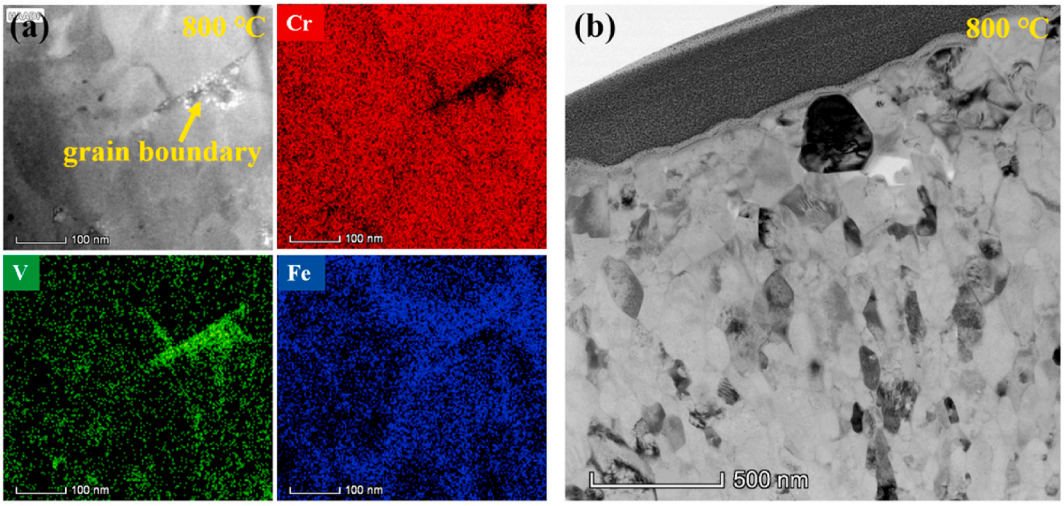

Fig. 12. (a) The cross-sectional STEM images of the wear track at 800 °C and the corresponding EDS mapping images of Cr, V and Fe. (b) The cross-sectional TEM bright field images of the oxide scale formed in wear track at 800 °C.

difference. Moreover, a loosened layer with laminated and multi-hole structures emerged between the oxide scale and the compacted coating. The melting of V_2O_5 reflected in the wear track morphology (Fig. 8c) further verified the scenario that the diffusion rate of vanadium at this temperature was limited and the compact structure obstructed deep oxidation of vanadium, and spallation of the coating in the wear track in Fig. 8c suggested that the oxide scale was brittle. So, the oxide scale was prone to fall off at a high shear strength during the sliding process at the oxide/coating interface. When the temperature increased to 800 °C, the thickness of the oxide scale soared to 1.6 μm, 10 times thicker than what was seen in case of 700 °C. Meanwhile, pores and voids among oxide grains were observed in the upper part of the oxide scale. The thicker oxide scale at 800 °C further reduced adhesion of asperity contacts, and the smeared morphology in the wear track

substantiated a soft V–O phase which provided adequate lubrication. The higher degree of oxidation with the increased temperature was regarded as a governing factor in the causation of lubrication behavior.

Although the presence of the oxide scale was benefit to the friction reduction, it was still unsatisfactory as it was developed at the expense of abrasion resistance [24]. Fig. 12b displays the magnified TEM picture of the oxide particulates at 800 °C. The oxide nanograins exhibited ambiguous poly facets morphology and grain refinement was evident at bottom of the oxide scale, while the apparent coarsening dominated the upper region, accompanying by the appearance of some pores and voids. The coarse grain at the sliding interface had poor deformability during the friction process, which progressively undermined oxide scale formability [27]. Herein, the oxide scale formed at 800 °C was vulnerability to damage. Compared with 700 °C, simultaneously, the (Cr, V)N coating oxidized at 800 °C had a greater degree of mechanical damage and exhibited poor wear resistance. At 900 °C, the degradation of the coating would cause its mechanical properties to collapse, and the coating was not equipped with wear resistance.

5. Conclusions

The $Cr_{0.58}V_{0.14}N_{0.28}$ coating with a V content of 14 at.% was deposited by a home-made cathodic arc evaporation system. In particular, we focused on the dependence of the high temperature tribological properties of the coating in range of 500–900 °C upon the oxidation behavior and mechanical properties after oxidation. It was found that the (Cr, V)N coating started to oxidize at 600 °C. As the temperature increased, the oxidation rate increased, and the coating undergone a transition from incomplete oxidation to complete oxidation. The structure became loose, which weakened the adhesion strength. The dissipation of the main phase of CrN also deteriorated the hardness of the coating. Therefore, the higher the oxidation temperature, the poorer the mechanical properties of the coating. Moreover, the evolution of high temperature tribological behavior of (Cr, V)N coating was divided into two stages. At 500–600 °C, the dynamic process of abrasive grain generation, powdering and self-aggregation led to a high coefficient of friction (0.57–0.63), and the damage of the adhesion strength at 600 °C reduced the wear resistance of the coating. At 700–900 °C, the degree of oxidation increased with increment of temperature, which promoting the formation rate of the soft V–O phase. As a consequence, the COF decreased significantly (0.28–0.37) and became lower and lower. However, the friction coefficient was reduced at the expense of wear behavior due to the consumption of V elements. In other words, as the temperature increased, the mechanical properties were damaged more seriously, causing the increased wear rate. The mechanical properties of the coating collapsed at 900 °C, and the wear resistance was fatally destroyed. In summary, the best tribological properties of the $Cr_{0.58}V_{0.14}N_{0.28}$ coating were obtained at 700–800 °C.

CRediT authorship contribution statement

Cuicui Wang: Conceptualization, Validation, Formal analysis, Investigation, Data curation, Writing – original draft, Visualization. **Beibei Xu:** Conceptualization, Investigation, Data curation, Writing – review & editing, Visualization, Project administration. **Zhenyu Wang:** Writing – review & editing, Project administration. **Hao Li:** Software, Resources, Project administration, Funding acquisition. **Li Wang:** Software, Investigation. **Rende Chen:** Software, Investigation. **Aiying Wang:** Investigation, Data curation, Writing – review & editing. **Peiling Ke:** Resources, Writing – review & editing, Visualization, Project administration, Funding acquisition.

Declaration of competing interest

The authors declare that they have no known competing financial interests or personal relationships that could have appeared to influence the work reported in this paper.

Acknowledgement

This research was supported by the National Natural Science Foundation of China (51875555, 52025014, 51901238), National Science and Technology Major Project (2017-VII-0013-0110), and Ningbo Municipal Natural Science Foundation (202003N4025).

References

[1] Wang ZY, Ke PL, Liu XC, Wang AY. Influence of substrate negative bias on structure and properties of TiN coatings prepared by hybrid HIPIMS method. J Mater Sci Technol 2015;31:37–42. https://doi.org/10.1016/j.jmst.2014.06.002.
[2] Drnovšek A, Rebelo de Figueiredo M, Vo H, Xia A, Vachhani SJ, Kolozsvári S, et al. Correlating high temperature mechanical and tribological properties of CrAlN and CrAlSiN hard coatings. Surf Coating Technol 2019;372:361–8. https://doi.org/10.1016/j.surfcoat.2019.05.044.
[3] Wang ZY, Li X, Wang X, Cai S, Ke PL, Wang AY. Hard yet tough V-Al-C-N nanocomposite coatings: microstructure, mechanical and tribological properties. Surf Coating Technol 2016;304:553–9. https://doi.org/10.1016/j.surfcoat.2016.07.061.
[4] Kumar DD, Kumar N, Kalaiselvam S, Dash S, Jayavel R. Wear resistant super-hard multilayer transition metal-nitride coatings. Surf Interfaces 2017;7:74–82. https://doi.org/10.1016/j.surfin.2017.03.001.
[5] Podgornik B, Sedlaček M, Mandrino D. Performance of CrN coatings under boundary lubrication. Tribol Int 2016;96:247–57. https://doi.org/10.1016/j.triboint.2015.12.039.
[6] Meng C, Yang L, Wu Y, Tan J, Dang W, He X, et al. Study of the oxidation behavior of CrN coating on Zr alloy in air. J Nucl Mater 2019;515:354–69. https://doi.org/10.1016/j.jnucmat.2019.01.006.
[7] Liu C, Bi Q, Matthews A. EIS comparision on corrosion performance of PVD TiN and CrN coated mild steel in 0.5 N NaCl aqueous solution. Corrosion Sci 2001;43:1953–61. https://doi.org/10.1016/S0010-938X(00)00188-8.
[8] Li W, Tang P, Shang L, He D, Wang L, Zhang G, et al. Tribological behaviors of CrN/Cr3C2-NiCr duplex coating at elevated temperatures. Surf Coating Technol 2019;378:124926. https://doi.org/10.1016/j.surfcoat.2019.124926.
[9] Lu C, Jia J, Fu Y, Yi G, Feng X, Yang J, et al. Influence of Mo contents on the tribological properties of CrMoN/MoS2 coatings at 25–700 °C. Surf Coating Technol 2019;378:125072. https://doi.org/10.1016/j.surfcoat.2019.125072.
[10] Polcar T, Martinez R, Vítů T, Kopecký L, Rodriguez R, Cavaleiro A. High temperature tribology of CrN and multilayered Cr/CrN coatings. Surf Coating Technol 2009;203:3254–9. https://doi.org/10.1016/j.surfcoat.2009.04.005.
[11] Xu BB, Guo P, Wang ZY, Chen RD, Ye YM, Shuai JT, et al. Anti-wear Cr-V-N coating via V solid solution: microstructure, mechanical and tribological properties. Surf Coating Technol 2020;397:126048. https://doi.org/10.1016/j.surfcoat.2020.126048.
[12] Franz R, Mitterer C. Vanadium containing self-adaptive low-friction hard coatings for high-temperature applications: a review. Surf Coating Technol 2013;228:1–13. https://doi.org/10.1016/j.surfcoat.2013.04.034.
[13] Klünsner T, Shen Q, Hlawacek G, Teichert C, Fateh N, Fontalvo GA, et al. Morphology characterization and friction coefficient determination of sputtered V2O5 films. Thin Solid Films 2010;519:1416–20. https://doi.org/10.1016/j.tsf.2010.09.040.
[14] Tillmann W, Sprute T, Hoffmann F, Chang Y-Y, Tsai C-Y. Influence of bias voltage on residual stresses and tribological properties of TiAlVN-coatings at elevated temperatures. Surf Coating Technol 2013;231:122–5. https://doi.org/10.1016/j.surfcoat.2012.03.012.
[15] Fateh N, Fontalvo GA, Gassner G, Mitterer C. Influence of high-temperature oxide formation on the tribological behaviour of TiN and VN coatings. Wear 2007;262:1152–8. https://doi.org/10.1016/j.wear.2006.11.006.
[16] Mayrhofer PH, Hovsepian PE, Mitterer C, Münz WD. Calorimetric evidence for frictional self-adaptation of TiAlN/VN superlattice coatings. Surf Coating Technol 2004;177–178:341–7. https://doi.org/10.1016/j.surfcoat.2003.09.024.
[17] Bobzin K, Bagcivan N, Ewering M, Brugnara RH, Theiß S. DC-MSIP/HPPMS (Cr,Al,V)N and (Cr,Al,W)N thin films for high-temperature friction reduction. Surf Coating Technol 2011;205:2887–92. https://doi.org/10.1016/j.surfcoat.2010.10.056.
[18] Mu Y, Liu M, Wang Y, Liu E. PVD multilayer VN–VN/Ag composite coating with adaptive lubricious behavior from 25 to 700 °C. RSC Adv 2016;6:53043–53. https://doi.org/10.1039/C6RA02370C.
[19] Cai Z, Pu J, Lu X, Jiang X, Wang L, Xue Q. Improved tribological property of VN film with the design of pre-oxidized layer. Ceram Int 2019;45:6051–7. https://doi.org/10.1016/j.ceramint.2018.12.076.
[20] Zhou Z, Rainforth WM, Lewis DB, Creasy S, Forsyth JJ, Clegg F, Ehiasarian AP, Hovespian PE, Münz WD. Oxidation behaviour of nanoscale TiAlN/VN multilayer coatings. Surf Coating Technol 2004;177–178:198–203. https://doi.org/10.1016/j.surfcoat.2003.09.031.
[21] Chang C-C, Chen H-W, Lee J-W, Duh J-G. Development of Si-modified CrAlSiN nanocomposite coating for anti-wear application in extreme environment. Surf Coating Technol 2015;284:273–80. https://doi.org/10.1016/j.surfcoat.2015.06.090.

[22] Lin J, Mishra B, Moore JJ, Sproul WD. A study of the oxidation behavior of CrN and CrAlN thin films in air using DSC and TGA analyses. Surf Coating Technol 2008; 202:3272–83. https://doi.org/10.1016/j.surfcoat.2007.11.037.
[23] Kinbara A, Baba S. Adhesion measurement of non-metallic thin films using a scratch method. Thin Solid Films 1988;163:67–73. https://doi.org/10.1016/0040-6090(88)90412-9.
[24] Kutschej K, Mayrhofer PH, Kathrein M, Polcik P, Mitterer C. Influence of oxide phase formation on the tribological behaviour of Ti–Al–V–N coatings. Surf Coating Technol 2005;200:1731–7. https://doi.org/10.1016/j.surfcoat.2005.08.044.
[25] Fateh N, Fontalvo GA, Gassner G, Mitterer C. The beneficial effect of high-temperature oxidation on the tribological behaviour of V and VN coatings. Eur Trans Res Rev 2007;28:1–7. https://doi.org/10.1007/s11249-007-9241-x.
[26] Luo Q. Temperature dependent friction and wear of magnetron sputtered coating TiAlN/VN. Wear 2011;271:2058–66. https://doi.org/10.1016/j.wear.2011.01.054.
[27] Tran BH, Tieu K, Wan S, Zhu H. Lubricant as a sticking-scale inhibitor on high temperature sliding contact. Tribol Int 2019;140:105860. https://doi.org/10.1016/j.triboint.2019.105860.